Wavelength Conversion for WDM Communication Systems Using Four-Wave Mixing in Semiconductor Optical Amplifiers

David F. Geraghty, Robert B. Lee, Marc Verdiell, Mehrdad Ziari, Atul Mathur, and Kerry J. Vahala, *Member, IEEE*

(Invited Paper)

***Abstract*—Four-wave mixing (FWM) in semiconductor optical amplifiers is an attractive mechanism for wavelength conversion in wavelength-division multiplexed (WDM) systems since it provides modulation format and bit rate transparency over wide tuning ranges. A series of systems experiments evaluating several aspects of the performance of these devices at bit rates of 2.5 and 10 Gb/s are presented. Included are single-channel conversion over 18 nm of shift at 10 Gb/s, multichannel conversion, and cascaded conversions. In addition time resolved spectral analysis of wavelength conversion is presented.**

***Index Terms*—Communication systems, frequency conversion, optical mixing, semiconductor optical amplifier.**

I. Four-Wave Mixing Wavelength Converters

A. Introduction

As NEW applications for telecommunications mature, such as HDTV, multimedia services, and the world wide web, greater demand is being placed on the bandwidth of the existing telecommunications systems. Single-mode fiber (SMF) installed around the world has the capacity of many Tb/s. Commercial high-speed systems operate in the range of 2.5–10 Gb/s, thus leaving much room for more efficient use of the available fiber bandwidth. Increasing the channel bit rate beyond current levels will prove to be increasingly difficult since the cost of the supporting electronics increases and the achievable transmission distance decreases due to fiber dispersion. Consequently, a world-wide consensus is driving the utilization of wavelength-division multiplexing (WDM) technologies for a more effective use of the available fiber bandwidth [1].

An important element for implementation of WDM systems is a wavelength converter [2], [3]. Many technologies exist for the implementation of wavelength conversion [4]. Optoelectronic, cross-gain saturation [5], and cross-phase saturation [6] wavelength converters are candidate technologies that offer excellent performance, however, they are not transparent to modulation format [7].[1] Complete or so-called strict transparency is offered only by ultra-fast wave mixing techniques based on either four-wave mixing (FWM) or difference frequency generation (DFG) [8]. DFG performance has made impressive strides in recent years through use of quasi-phase matching in AlGaAs waveguides [9]. However, the use of quasi-phase matched waveguides mandates a fixed pump wavelength. This, in turn, means that a given input wavelength can be mapped to only one converted wavelength. FWM in optical fibers [10] is limited by this same pump wavelength restriction. On the other hand, FWM in semiconductor optical amplifiers (SOA's) [11]–[44] is insensitive to phase matching, offering arbitrary wavelength mapping. Offsetting this advantage are disadvantages associated with polarization dependent conversion as well as the required output filtering of spurious wavelengths. Nonetheless, FWM SOA wavelength converters have demonstrated high bit rate switching between WDM channels [14], [15], [24], dispersion compensation by phase conjugation (or mid-span spectral inversion) [16], [19], time-domain demultiplexing [40], multiplexing format conversion, [41], wavelength conversion of microwave subcarriers [42], and also limited signal processing [43], [44]. In particular, optical signal-to-noise ratio (OSNR), once considered the primary obstacle to any progress toward application of these devices has improved dramatically over the last year and further improvements seem likely.

Fig. 1(a) is a schematic for a typical FWM experimental configuration. Two copolarized waves are coupled into the SOA. One of the waves, called the pump wave (E_p) with frequency ω_p, is typically stronger than the other wave (i.e., the input signal to be converted) called the probe wave (E_q) with frequency ω_q. Inside the SOA, the copropagating pump and probe waves mix, forming dynamic gain and index gratings in the SOA through the mechanisms of carrier density modulation, carrier heating and spectral hole burning. The pump wave scattering from these gratings generates two waves, one at the probe frequency and one at a new frequency, $\omega_{cs} = 2\omega_p - \omega_q$. Probe scattering also generates two much weaker waves, one at the pump frequency and one at $\omega_{cs'} = 2\omega_q - \omega_p$. The wave E_{cs} with frequency ω_{cs} is easily shown to be the phase conjugate replica of the original input

Manuscript received June 4, 1997; revised September 12, 1997. This work was supported by ARPA under Contract DAAL 01-94-K-03430 and the National Science Foundation under Grant ECS-9412 862.

D. F. Geraghty, R. B. Lee, and K. J. Vahala are with the Department of Applied Physics, California Institute of Technology, Pasadena, CA 91125 USA.

M. Verdiell, M. Ziari, and A. Mathur are with SDL, San Jose, CA 95134 USA.

Publisher Item Identifier S 1077-260X(97)09137-5.

[1] Strictly speaking, these techniques are not transparent to bit rate, however, recent results at 40 Gb/s show they have an "effective" bit rate transparency.

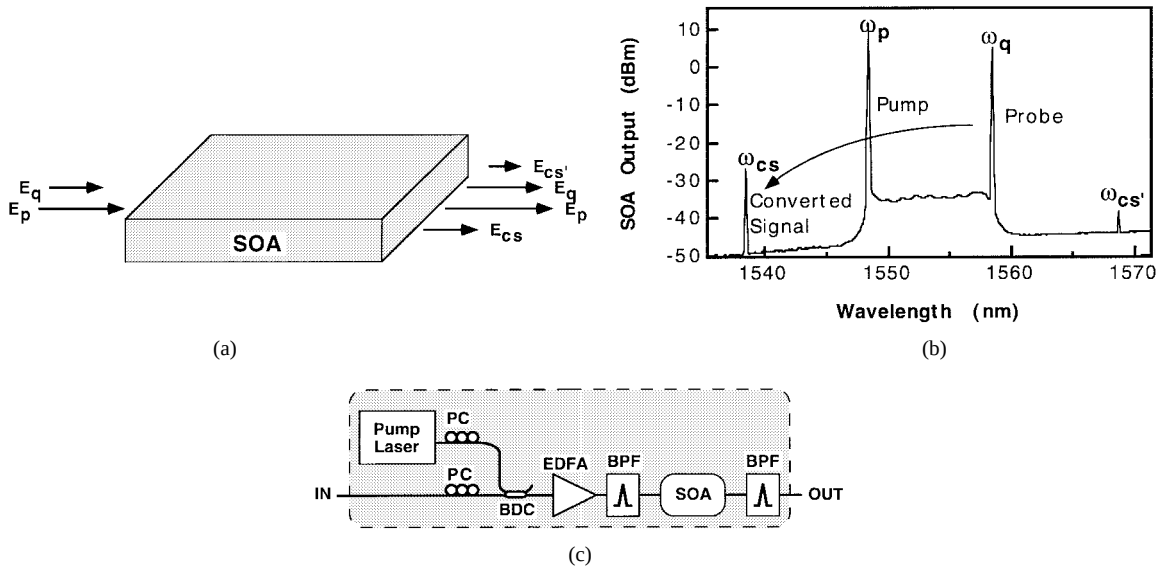

Fig. 1. (a) Experimental configuration for single-pump FWM. (b) Typical SOA output spectra with 1 Å bandwidth resolution; SOA input has pump-to-probe ratio of 5.6 dB and provides a 20-nm downshift. (c) Schematic of wavelength converter design.

signal. As such, it provides the wavelength converted signal. In this paper, we will provide a review of our recent results concerning the application of SOA-based four-wave mixing to wavelength conversion of high bit rate base-band digital optical signals.

A general block diagram for the wavelength converter used in the experiments described below is shown in Fig. 1(c). The converter's optical pump source is a tunable, external-cavity diode laser. Its in-fiber output power is about +3 dBm. The pump and probe waves each pass through individual polarization controllers (PC's) before being combined by an 80/20 bidirectional coupler (BDC). The combined signals are then amplified in a high power erbium-doped fiber amplifier (EDFA), with an output power of about +19 dBm. After amplification, the signals pass through a 10-nm-wide bandpass filter (BPF). As described in [28], [29], this filter increases the OSNR of the converted signal by suppressing the amplified spontaneous emission (ASE) contributed by the high-power EDFA in the spectral region of the converted signal. Following this ASE prefiltering, these signals are coupled into the SOA where FWM generates the converted signal. The SOA is a fiber pigtailed unit from SDL based on a multiquantum-well compressively strained gain medium providing 25-dB fiber-to-fiber gain. A typical FWM spectral output for this setup is shown in Fig. 1(b). After mixing in the SOA, the pump and the original signal are suppressed using a 1-nm-wide tunable bandpass filter centered on the converted signal.

B. Performance Characterization

The most frequently cited figures of merit for FWM wavelength converters are their conversion efficiency and the converted OSNR. The conversion efficiency is defined as the in-fiber converted signal power at the SOA output divided by the in-fiber signal power at the SOA input and has been accurately modeled and thoroughly characterized [11]–[13], [31]–[39]. However, from a systems perspective, the conversion efficiency is not the primary figure of merit. By using EDFA's in appropriate positions, it is possible to attain nearly any desired conversion efficiency. The more crucial figure of merit is the OSNR for the converted signal. Its importance is particularly significant to the optimization of a given SOA FWM element for wavelength conversion, because optimum OSNR does not necessarily imply optimum conversion efficiency [20]. This is true because whereas the amplification intrinsic to the SOA FWM element benefits the conversion efficiency, it also degrades the OSNR through generation of ASE in the converted signal band. This can be seen in Fig. 2(a) and (b) which show measured conversion efficiency and OSNR (wavelength down-shift of 6 nm and 1 Å optical bandwidth) versus the total SOAinput power. It can be seen that with increasing input power, and hence increased SOA saturation, conversion efficiency decreases while OSNR steadily rises. As such, it is always better to operate the SOA FWM element in deep saturation to attain maximum OSNR. This will be the case for all experiments described below. Typical total SOAinput power levels will be in the range of 12 dBm and will be boosted to this level using the high-power EDFA in Fig. 1(c). In addition, as described above, an ASE prefilter is used to strip the ASE spectral components generated by this EDFA within the conversion band. This prefiltering typically results in an added 5 dB of OSNR.

Other factors can also influence the magnitude of the OSNR: saturation power, gain, interaction length, and strength of the contributing nonlinear mechanisms. Assuming SOA operation in deep saturation as a given, the OSNR attainable with a fixed SOA structure is then primarily determined by two operating parameters: the wavelength shift and the pump-to-probe ratio. This dependence is illustrated in Fig. 2(c) and (d). Fig. 2(c) shows the measured converted signal power as a function of the wavelength shift. This wavelength dependence can be understood by modeling the various ultrafast dynamics that contribute to the nonlinear susceptibility function of the amplifier. In particular, the converted signal power at the SOA

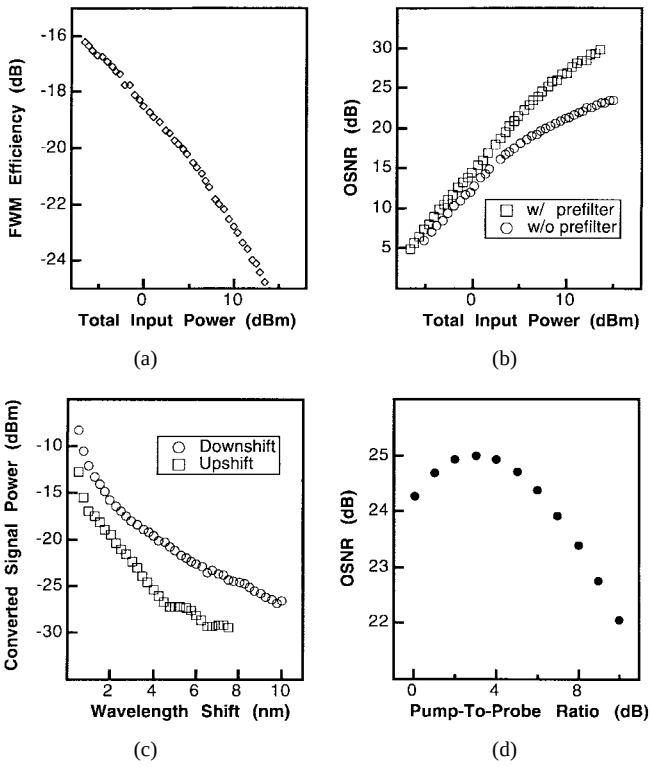

Fig. 2. (a) Measured conversion efficiency as a function of the total SOAinput power. (b) Measured OSNR (into 1-Å bandwidth) as a function of the total SOA input power, both with and without an ASE prefilter. (c) Measured converted signal power as a function of wavelength shift. (d) Predicted OSNR (into 1-Å bandwidth) as a function of the pump-to-probe ratio.

output is given approximately by [11]–[13], [35]

$$E_{cs} = E_q^* E_p^2 \left[\frac{A_{cd} e^{i\phi_{cd}}}{1 - i\Omega\tau_s} + \frac{A_{ch} e^{i\phi_{ch}}}{(1 - i\Omega\tau_{ch})(1 - i\Omega\tau_{sh})} + \frac{A_{sh} e^{i\phi_{sh}}}{1 - i\Omega\tau_{sh}} \right] \quad (1)$$

where E_q and E_p are the unconverted signal and the pump at the SOA input, respectively, $\Omega = \omega_p - \omega_q$ is the detuning frequency, and A_i, ϕ_i, and τ_i are the magnitudes, phases and time constants associated with the contributing ultrafast mechanisms where $i = cd$ (carrier density modulation), ch (carrier heating) and sh (spectral-hole burning). Many of these parameters will in general depend on the overall saturation level of the SOA. In the current experiment, they can be regarded as approximately constant since the total SOA input power is approximately fixed, due to the high level of saturation of the high-power EDFA shown in Fig. 1(c). As such, the overall rolloff in the converted power (and hence efficiency and OSNR) apparent in Fig. 2(c) reflects the superposition of the three response functions in the above equation. In addition, the asymmetry in the up and down conversion response results from partially destructive/constructive phase interference between the contributing FWM mechanisms for wavelength upshifts/downshifts.

The pump-to-probe (P/Q) ratio is important for several reasons. First, since FWM results from a third-order nonlinearity, the theoretically optimum P/Q ratio at constant total power is 3 dB. This is illustrated in Fig. 2(d) which shows the predicted OSNR into a 1-Å bandwidth as a function of the P/Q ratio for a wavelength downshift of 16 nm. Second, the P/Q ratio establishes the magnitude of the probe relative to the SOA saturation power. This is true because in deep saturation, the SOA gain saturation characteristic has an effective saturation power that approaches the total input power to the device (in the present case this is approximately the input pump power). As such, the P/Q ratio gives an approximate measure of parasitic gain saturation induced by the input signal. Such parasitic saturation can degrade the converted signal through intersymbol interference (ISI) and chirping that accompanies modulation in the modal gain of the SOA.

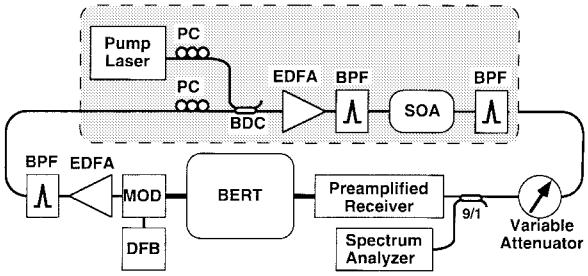

Fig. 3. Experimental setup for single-channel wavelength conversion.

II. Single-Channel Wavelength Conversion

Although FWM in semiconductor SOA's is a promising mechanism for wavelength conversion, there are many parameters that must be characterized and optimized for the converter to be usefully implemented. The device must be able to convert over a wide wavelength range. Conversion over the entire EDFA gain bandwidth is optimal, however, conversion over 10–20 nm is sufficient for most near term WDM applications. The spectral range will be determined by the OSNR of the converted signal, with increasing shifts resulting in lower OSNR's. Ideally, the device should also be able to accommodate a wide range of input signal powers. This dynamic input range will be determined by performance dependence on the P/Q ratio.

A. Experimental Setup

The experimental setup is shown in Fig. 3. Signal generation, error detection, and eye diagram analysis are done using a 10-Gb/s bit-error-rate tester (BERT) and a microwave transition analyzer. The optical signal source, the probe, is a distributed feedback (DFB) laser whose output is modulated at 10 Gb/s with a nonreturn-to-zero (NRZ) pseudorandom bit stream (PRBS) by a $LiNbO_3$ Mach–Zehnder external modulator. To compensate for losses in the modulator, it is followed by an EDFA-BPF pair. This signal is then input to the wavelength converter.

Following the wavelength converter is a variable attenuator and a tap. This allows us to take BER versus received power data. The attenuated signal is then detected by a preamplified receiver. The preamplified receiver has a high-gain, low-noise EDFA at its input with a wavelength dependent gain varying from 30–40 dB. Due to this spectral dependence and the use of a fixed wavelength signal source, we are unable to provide

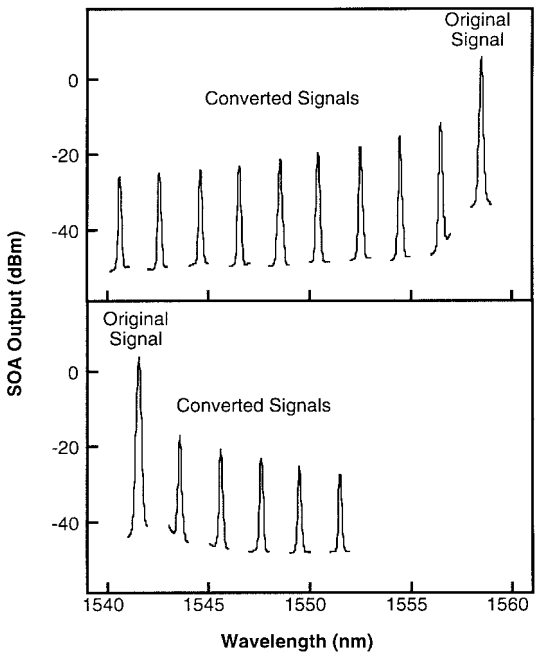

Fig. 4. Probe and converted signal spectra at SOA output for shifts up 2–18 nm and down 2–10 nm.

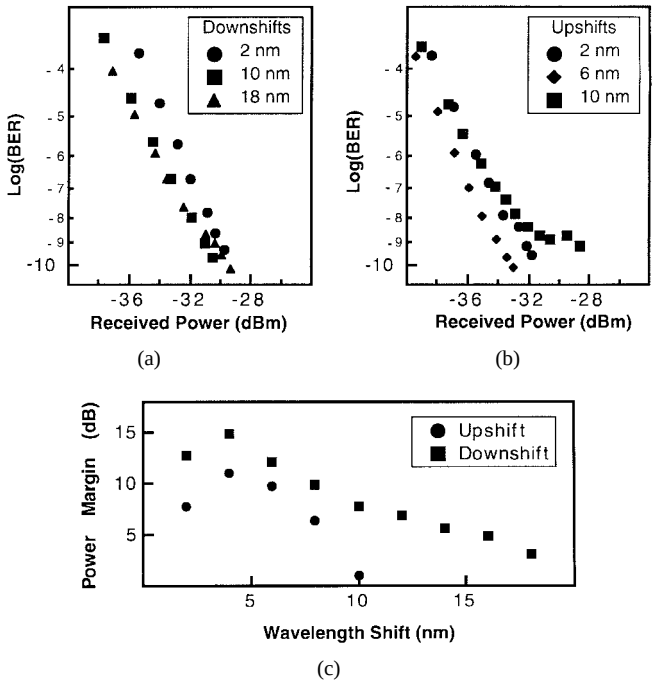

Fig. 5. (a) BER versus received power data for the downshifts at 10 Gb/s. (b) BER versus received power data for the upshifts at 10 Gb/s. (c) Power margin for converted signals as a function of shift.

baselines (unconverted signal BER performance) to compare with the performance of the signal after a single conversion.

The preamplifier EDFA is followed by a 1-nm-wide tunable bandpass filter. The optically amplified signal is then detected and electrically amplified with a Hewlett-Packard lightwave converter (a PIN receiver followed by an electrical amplifier). High frequency noise is suppressed by the rolloff of the electrical amplifier gain for the 10-Gb/s experiments, and by a standard SONET filter for experiments at 2.5 Gb/s. This receiver output is then split by a $10\times$ coaxial probe at the BERT input in order to facilitate both eye diagram and BER measurements.

B. Performance Dependence on Wavelength Shift

The versatility in choice of wavelength shift is one of the attractive features of FWM in SOA's (as compared to DFG). Large shifts of up to 75 nm have been measured [13], [22], however, as mentioned earlier, efficiency and OSNR degrade with increasing detuning. Ultimately, the BER begins to seriously degrade beyond some maximum detuning. A wavelength converter in a WDM system must be able to convert between any of the system's channels. Sufficient proof of this capability is demonstrated by accessing the entire spectral region spanned by the WDM channels from the edges of the channel spectrum, i.e., upshifting from the lowest channel and downshifting from the highest channel. In this section, we investigate the maximum conversion range that is compatible with a certain error rate using the SOA devices described above.

Beginning with a probe signal at 1558.5 nm, the converter is characterized for downshifts every 2 nm from 2 to 18 nm. For the SOA studied here, BER performance $<10^{-9}$ was not obtainable for downshifts of 20 nm and greater. The spectra of the original signal and the converted signals at the output of the SOA are shown in the upper panel of Fig. 4. At a 2-nm shift, the converted signal is 17.9 dB down from the original signal measured at the SOA output. This value decreases to 31.7 dB down for the 18-nm shift. The background ASE in the spectral region of the converted signals is approximately constant due to the constant total input power for the various shifts. The ASE level rises slightly for the 2-nm shift due to incomplete suppression of the high-power EDFA ASE by the prefilter. The resulting converted signals have OSNR's ranging from 32 to 24 dB into a 1-Å bandwidth.

BER versus received power data were taken for each of the above shifts. The data presented was taken for PRBS 2^7-1, however, the performance exhibited minimal pattern dependence ($<$0.5 dB) for pattern lengths up to PRBS $2^{31}-1$. The BER curves for shifts of 2, 10, and 18 nm are shown in Fig. 5(a). For the 2-nm shift, a second bandpass filter is used in series at the converter output to more fully suppress the pump. The curve for the 18-nm shift has two features of note. There is a slight flooring at small BER due to the decreased OSNR of the converted signal. Also, BER's $>10^{-7}$ actually occur at smaller received power levels than for similar BER's at smaller shifts having larger OSNR's. This results from spectral variation in the performance of the receiver.

Beginning with a probe signal at 1541.5 nm, the converter performance was also characterized for upshifts every 2 nm from 2 to 10 nm. BER performance $<10^{-9}$ was not obtainable for upshifts of 12 nm and greater. Original signal and converted signal spectra are shown in the lower panel of Fig. 4. The reduced efficiency for the upshifts is evident, with the converted signal down 21.0 dB at the 2-nm shift and falling to 31.1 dB down at the 10-nm shift. Again, the background ASE is approximately constant, rising slightly for the 2-nm shift. The resulting OSNR's range from 27.1 to 20.5 dB into 1-Å

bandwidth. BER versus received power data are again taken for each shift. The curves for shifts of 2, 6, and 10 nm are shown in Fig. 5(b). The curves display characteristics similar to those for downshifts, with the flooring at low BER for the largest shift much more evident.

In characterizing the capability for shifts both up and down in wavelength, complete coverage of a 10-nm range by our wavelength converter has effectively been demonstrated. Although not presented here, a similar experiment using a DFB laser directly modulated at 2.5 Gb/s as the optical signal source has also been performed. With this input signal, the wavelength converter demonstrated complete coverage of a 16-nm range. Finally, we note that in practice some margin would be required if these devices were to be used in an actual system. This would reduce the range of wavelength coverage. Fig. 5(c) shows the measured margin versus wavelength shift for this measurement where margin is defined as the converted signal attenuation required to degrade the BER to 10^{-9}.

C. Pump-to-Probe Ratio

The dependence of the dc conversion efficiency on the P/Q ratio is well understood, with a 3-dB ratio being optimal for maximum efficiency at fixed total input power. However, it has previously been shown that this ratio is not optimal for the case of a modulated input signal [21]. Modulating a high percentage of the input power to the SOA can induce modulation of the SOA gain and cause ISI. To date, most reported experiments have simply maintained a large P/Q ratio and mentioned the possibility of this problem [14], [18]. In this section, we investigate the effect of P/Q ratio on the performance of the wavelength converter. Before proceeding, we remind the reader that the utility of the P/Q ratio as a parameter requires that the SOA be operated in deep saturation.

To achieve varying P/Q ratio values, the input signal power to the wavelength converter is varied. This maintains the overall dc input power to the SOA approximately constant, due to the high level of saturation of the high-power EDFA preceding the SOA. The dc P/Q ratio was varied from 4.7 to 20 dB, with the wavelength shift kept constant at 9-nm downshift. The setup for this experiment is identical to that shown in Fig. 3 except for a variable attenuator introduced at the wavelength converter input to vary the P/Q ratio, and use of a DFB laser directly modulated at 2.5 Gb/s. This data rate is selected to enable comparison of the data with that for the multichannel results that will be presented in Section III-B.

BER versus received power data was taken for multiple patterns, PRBS 2^7-1 and PRBS $2^{31}-1$. The BER curves for P/Q ratios of 4.7 and 20 dB are shown in Fig. 6(a). The curves for P/Q $= 4.7$ dB show linear performance with only a minimal pattern dependence. However, the curves for P/Q $= 20$ dB show degraded performance, with the curves shifted to slightly higher powers and some flooring evident at the smallest BER values (this results from the reduced OSNR of the converted signal). Again, there is only a slight pattern dependence to the performance, with PRBS $2^{31}-1$ yielding a small degradation. The longer patterns contain longer strings of "1's" and "0's," allowing for more complete saturation of the SOA gain and hence the possibility of more ISI.

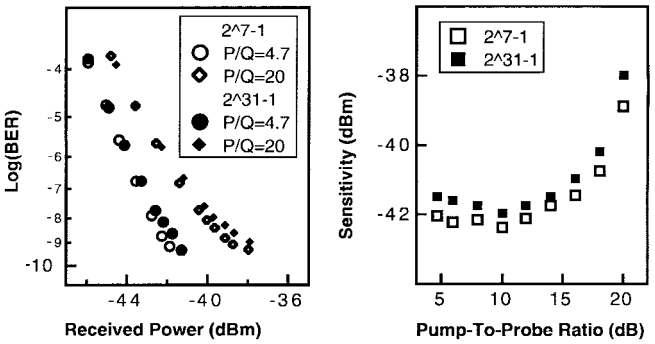

(a) (b)

Fig. 6. (a) BER versus received power data for the various P/Q ratios at 2.5 Gb/s. (b) Sensitivity versus P/Q ratios for single-channel operation at 2.5 Gb/s.

To further quantify the performance we define the sensitivity as the received power required for a BER of 10^{-9}. The sensitivity as a function of the P/Q ratio is shown in Fig. 6(b). For a high P/Q ratio, the converted signal power is low, yielding a reduced OSNR at the SOA output. In this case, the BER versus received power curves exhibit flooring, thereby degrading the sensitivity. As the P/Q ratio decreases to 10 dB, the converted signal power and the OSNR increase. The higher OSNR eliminates the flooring in the curves and the sensitivity improves. As the P/Q ratio decreases further, the optical pump power begins to decrease due to cross gain saturation in the high power EDFA and in the SOA itself. For the small P/Q ratios, this causes the sensitivity to flatten out. This flattening is slightly more than would be predicted based on modeling EDFA and SOA gain saturation and might also be the effect of ISI caused by fluctuations in the saturation of the SOA.

Similar to Summerfield and Tucker [21], we have found that operating at a P/Q ratio of 3 dB is not optimal. The converter shows relatively flat, consistent performance for P/Q ratios ranging from about 5–15 dB or equivalently a dynamic input power range of about 10 dB. This is similar to the results of [21], shifted to smaller P/Q. Additionally, the performance of the converter is relatively independent of the pattern length, with minimal degradation resulting from increasing the pattern length from 2^7-1 to $2^{31}-1$.

III. Multichannel Operation

One advantage of wavelength conversion by FWM is the potential to perform conversion of multiple channels simultaneously without first using demultiplexing equipment to separate the incoming signals. This can simplify, for example, dispersion compensation in WDM systems by mid-span optical phase conjugation. However, simultaneous conversion does present the opportunity for crosstalk between the signals [17]–[19]. The magnitude of this crosstalk is determined approximately by the P/Q ratio and is experimentally investigated in this section.

A. Experimental Setup

The setup for this experiment is identical to the setup shown in Fig. 3, except that in this experiment we begin with two probe signals provided by two DFB lasers directly modulated

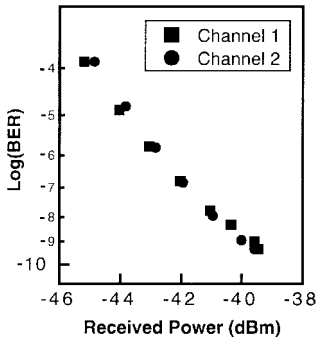

(a)

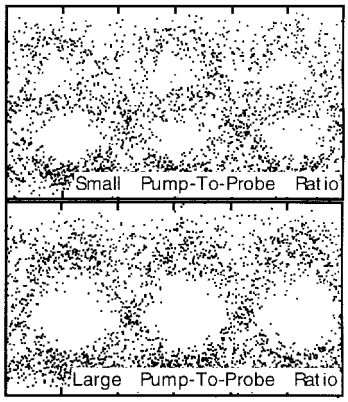

(b)

Fig. 7. (a) BER versus received power data for both channels of a multichannel converter at 2.5 Gb/s with P/Q = 16 dB. (b) Detected eyes for dual channel operation at 2.5 Gb/s with small (7.4 dB) and large (16 dB) pump-to-probe ratios.

at 2.5 Gb/s using complementary data patterns. To decorrelate the data on the two channels, the signals propagate through different lengths of fiber before being combined in a 50/50 BDC and then input to the wavelength converter. The signals were separated in wavelength by 1.5 nm. Signal power levels were adjusted so as to give identical P/Q ratios at the SOA output. The selected pump wavelength provided 6 and 9 nm downshifts for the inner and outer channel, respectively.

B. Multichannel Performance

By maintaining a large P/Q ratio, the input signals do not significantly contribute to the gain saturation of the high-power EDFA and the SOA, and simultaneous wavelength conversion of both channels is possible. Fig. 7(a) shows the BER performance of two channels converted at a P/Q ratio of 18 dB. Both channels show a linear BER performance with identical sensitivity and only modest flooring.

This performance was only attainable for a large P/Q ratio. Through the mechanism of cross-gain saturation in the SOA, both a signal and the noise it carries can be impressed on the pump wave. This effect worsens with decreasing P/Q ratio and can be easily observed in the conversion of a single channel. For example, with P/Q ratios of <5 dB, cross-gain saturation is so effective that it is possible to attain BER $<10^{-9}$ by detecting the inverted signal that has been imprinted on the pump. In two channel conversion, this process can impose the signal and the noise of one channel onto the converted signal of the other channel. This is evident in the eye diagram shown in the upper panel of Fig. 7(b), taken during multichannel operation with a P/Q ratio of 7.4 dB. Here, we see that the eye has two "1" levels; the higher and lower "1" level corresponding to when the channel not being detected is "0" and "1," respectively.

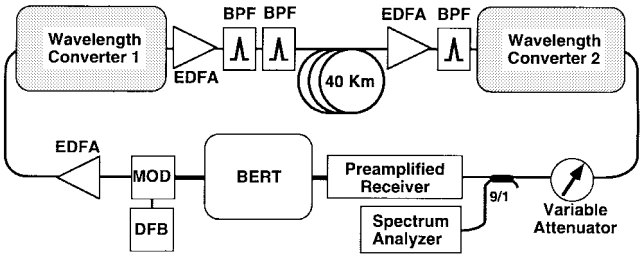

Fig. 8. Experimental setup for cascaded wavelength conversions at 10 Gb/s.

For larger P/Q ratios, the contribution to gain saturation by the input signals is negligible and the eye diagrams show no evidence of dual "1" levels. This can be seen in the eye pattern shown in the lower panel of Fig. 7(b), taken for a P/Q ratio of 16 dB. For this P/Q ratio, the sensitivity under multichannel operation is within 0.5 dB of the sensitivity under single-channel operation at the same P/Q ratio. For the wavelength converter of this study, the sensitivity of the converted signal under multichannel operation began to degrade, compared to single-channel operation, for a P/Q less than 15 dB. The exact point at which degradation occurs, however, will depend on several factors and this value should not be taken as a fundamental limit.

IV. CASCADABILITY

With wavelength converters as the interconnection elements between levels in a WDM system, a signal traveling between multiple levels would be required to undergo multiple conversions. Consequently, implementation of converters in scalable WDM networks will require converters with sufficient OSNR for cascading. In this section we review recent results on the first demonstration of cascaded wavelength conversion by FWM in an SOA [25].

A. Cascaded Wavelength Conversions

The system used to investigate cascadability of wavelength converters is shown in Fig. 8. The pump wave for both converters is provided by the same laser, split in a 50/50 BDC. This allows our cascaded converters to shift the signal down in wavelength and then back up to the original wavelength. Doing this, we are able to accurately compare the twice-converted signal performance to that of the original signal as both signals will be at the same wavelength (and hence will see the same preamplified receiver performance).

The cascade system performance is evaluated at multiple points in the system. First, a back-to-back baseline analysis of the original, unconverted signal is performed. Next, the performance of the first converter is characterized by detecting the signal at its output. Finally, the twice-converted signal

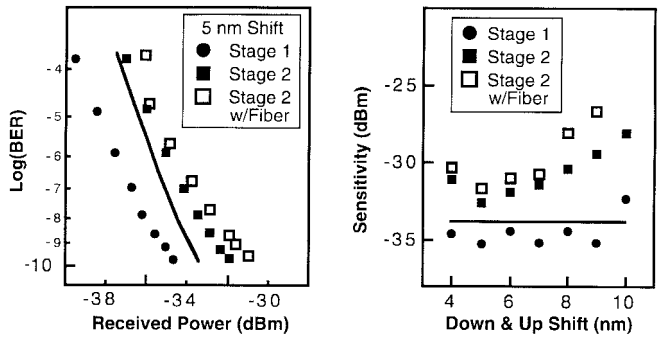

(a) (b)

Fig. 9. (a) BER versus received power data at various points in the cascaded system at 10 Gb/s for down and up shifts of 5 nm. (b) Sensitivity at multiple points in the cascaded system at 10 Gb/s as a function of wavelength shift.

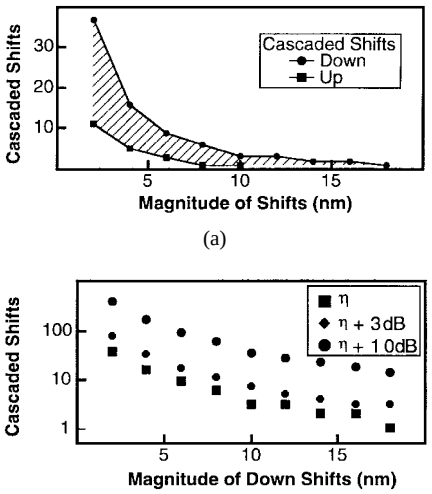

(a)

(b)

Fig. 10. (a) Predicted limits of cascaded shifts monotonically down, up and varying in wavelength. (b) Predicted cascadability improvements resulting from conversion efficiency improvements.

is characterized both with and without a 40-km link of fiber followed by an EDFA and a bandpass filter to compensate for propagation losses.

The results for a 5-nm shift down and then up are shown in Fig. 9(a). Performance after the first wavelength converter is improved relative to the baseline. This results primarily from the converted signal wavelength seeing an improved preamplified receiver performance relative to the original signal wavelength. After the second conversion, comparison of the twice converted signal with the original signal shows minimal degradation of performance. The sensitivity is within 2 dB of the original, unconverted signal. The addition of the 40-km span of fiber causes a small degradation of the performance.

This characterization was repeated for down and up shifts from 4 to 10 nm. The measured sensitivity, again defined as the received power required for a BER of 10^{-9}, is presented in Fig. 9(b). The rise in the sensitivity at the shortest shifts is due to incomplete suppression of the pump at the output of the first converter. This was observed to generate noise through an interferometric effect with the pump in the second converter. This could be avoided by using an improved bandpass filter.

B. Predicted Limits

Experimentally, we are limited by available equipment to demonstrating two cascaded FWM SOA wavelength converters. However, using the converter's measured conversion efficiency and OSNR, shown in Fig. 4, the limits of the cascadability for the converter tested here can be modeled [26]. In the model, each converter is followed by an EDFA in order to boost the power of the converted signal to a level high enough to be input into the subsequent converter. The amplified converted signal is then attenuated to $+3$ dBm. This power level yields a P/Q ratio of 6 dB, matching the P/Q ratio used in measuring the conversion efficiencies and OSNR.

A few simple approximations are made to facilitate modeling. The background ASE spectrum generated by the SOA is assumed to be flat and therefore shift independent. Additionally, the performance of the EDFA's is assumed to be spectrally independent. The assumed background ASE level of -49.25 dBm into 0.1-nm bandwidth and the assumed EDFA performance of 33-dB gain with 4.5-dB noise figure are set by the measured performance of our equipment.

Using these values, the OSNR is calculated until the resulting OSNR falls below that required for 10^{-9} BER upon detection. For the purpose of illustration, this defines the cascade limit of the wavelength converter. It should be noted that this model does not take into account any additional BER performance degradation that may occur from signal distortion or extinction ratio degradation.

The predicted cascadability of the converter is shown in Fig. 10(a). The number of cascaded shifts possible is calculated for shifts of equal magnitude down and up in wavelength. Up to 37 downshifts of 2 nm are possible. This rapidly drops to only 3 downshifts at 10 nm per shift. The 18-nm downshift is not cascadable. The reduced conversion efficiency for wavelength upshifts results in reduced cascadability for repeated upshifts. Only 11 upshifts of 2 nm are possible, and the converter is not cascadable for upshifts of 8 nm and greater. Alternating between shifts up and down in wavelength provides intermediate cascadability performance, indicated by the shaded region.

Possibly the most useful result of this model is the ability to predict the improvement in the cascadability that could result from improved conversion efficiency and OSNR. Increased efficiencies could result from improvements in the SOA design, such as increased saturation power or increased length. Fig. 10(b) compares the cascadability for repeated downshifts for the converter of this study with that for hypothetical converters providing conversion efficiencies that are 3 and 10 dB greater. The number of cascaded shifts possible is almost directly proportional to the conversion efficiency.

V. Time Resolved Spectral Analysis

Most of the optical fiber utilized world-wide is nondispersion shifted fiber, with its zero dispersion point near 1.3 μm. The successful development of EDFA's has mandated the use of 1.55-μm lasers for long-haul links. With EDFA's properly

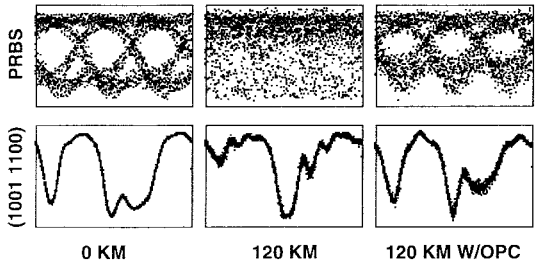

Fig. 11. 10-Gb/s eye diagrams at 0 km, 120 km without mid-span phase conjugation, and 120 km with optical phase conjugation.

placed in the link, the primary factor limiting achievable transmission distance becomes signal distortion due to chromatic dispersion from propagation in the optical fiber. Intrinsic to the process of wavelength conversion by FWM is optical phase conjugation of the input signal. Yariv *et al.* [45] proposed optical phase conjugation to compensate for chromatic dispersion in single-mode fiber. Demonstrations have utilized both SOA [16] and fiber [46], [19] FWM wavelength converters to perform the optical phase conjugation with impressive results.

We have performed optical phase conjugation on a 10-Gb/s signal over 120 km of standard, nondispersion shifted fiber. The eye diagrams are shown in Fig. 11. For 120-km transmission with mid-point optical phase conjugation, the eye diagrams show fairly accurate regeneration of the original signal. There is some additional noise, due to OSNR degradation induced by the EDFA's and the wavelength converter, but we are still able to perform error-free detection at 10 Gb/s for over 2 min. In addition to the extra noise, there is a some minor distortion of the original signal. This most likely indicates nonideal phase conjugation by the wavelength converter, resulting from additional chirp introduced by the converter and discussed below. The magnitude of this additional chirp is dependent upon the P/Q ratio, which determines the modal gain fluctuations that occur. Below, we investigate this chirp and its dependence on P/Q ratio using the technique of time-resolved spectral analysis.

A. Experimental Setup

To evaluate the performance of FWM SOA wavelength converters as optical phase conjugators and to also gain information on the presence of parasitic chirp upon conversion, we have performed time resolved spectral analysis (TRSA). This technique has previously been used for evaluating the spectral characteristics of modulated lasers [47]. By passing the signal through a narrow bandpass filter before detection, the signal's spectral shape can be determined as a function of time. In this paper, TRSA is performed on 10-Gb/s signals, both unconverted and converted, that have been generated by a directly modulated DFB laser. The narrow bandpass filter utilized is a Hewlett-Packard optical spectrum analyzer with an optional optical output port. It's bandwidth of 0.8 Å is not optimal, but provides superior stability. The center wavelength of the filter is stepped by 0.05 Å over the entire spectral width of the signal for each measurement. The filtered signals are then detected for each step, using the preamplified receiver described above but without the electrical amplifier. The signals are then input to a microwave transition analyzer from which data is gathered and processed using a LABVIEW program. The pump laser wavelength of the converter is set to provide a 6-nm shift.

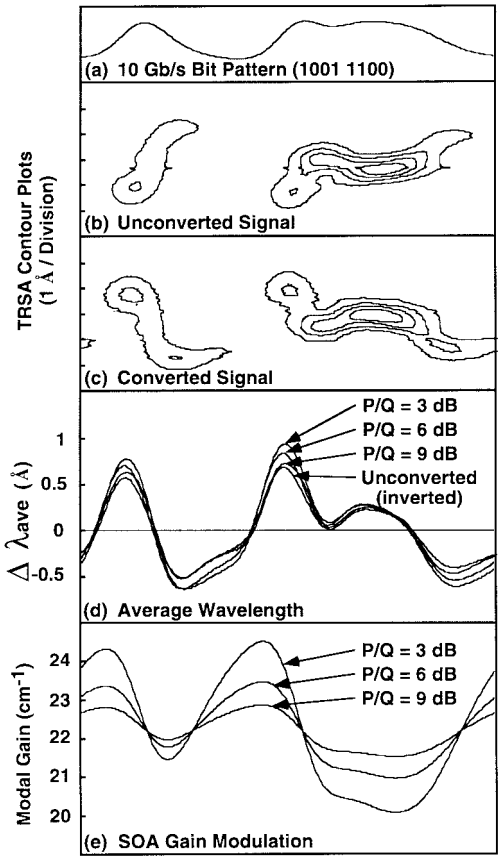

Fig. 12. Time resolved spectral analysis of both the input signal and the converted signal. at 10 Gb/s. (a) The complete 10-Gb/s bit pattern. (b) The unconverted and (c) the converted signal contour plots of constant power with time and frequency as the x- and y-axis, respectively. (d) The measured average wavelength of the unconverted signal (inverted) and the converted signal for a P/Q ratios of 3, 6, and 9 dB. (e) Predicted SOA gain fluctuations for P/Q ratios of 3, 6, and 9 dB.

B. Additional Chirp

TRSA was first performed on multiple patterns with a P/Q ratio of 6 dB. The results of the analysis for the pattern (1001 1100) are shown in Fig. 12. Fig. 12(a) shows the complete, unfiltered bit pattern. Fig. 12(b) and (c) shows TRSA contour plots of constant power for both the unconverted and the converted signals with time and wavelength as the x and y axes, respectively. These plots clearly illustrate the spectral inversion resulting from the optical phase conjugation that is intrinsic to the FWM process. Also apparent is an increase in the spectral width of the converted signal.

For a more quantitative analysis, the average wavelength was calculated for each point in time [48]. For the pattern presented, the spectral width increased by 0.27 Å, or 23%, upon wavelength conversion. For all the patterns tested at a P/Q ratio of 6 dB, the span increased between 0.05 and 0.5

Å, or 6 to 44%. The magnitude of the increase was found to depend on the P/Q ratio. The measured average wavelength of a (1001 1100) pattern for P/Q ratios of 3, 6, and 9 dB is shown in Fig. 12(d). The average wavelength span increases by 0.38, 0.27, and 0.054 Å, or by 31.5%, 22.8%, 4.5%. Also shown is the average wavelength of the unconverted signal (inverted for easy comparison).

This additional chirp is introduced primarily by parasitic signal modulation of the SOA gain. Ignoring the transit time of the signal in the SOA and assuming a spatially independent gain, a simple analysis of signal amplification yields the equations [49]

$$\frac{dg}{dt} = \frac{g_0 - g}{\tau_s} - \frac{g}{\tau_s}\left[\frac{P}{P_{\text{sat}}}\right]^{1.2}$$
$$\frac{d\phi}{dt} = -\frac{1}{2}\alpha\frac{dg}{dt}L \tag{2}$$

where g is the modal gain, g_0 is the small-signal modal gain, τ_s is the spontaneous lifetime, P is the total power in the SOA, P_{sat} is the saturation power of the SOA, ϕ is the phase of the signal, α is the linewidth enhancement factor, and L is the length of the SOA. The exponent of 1.2 has been added to the gain saturation term to more accurately match the measured saturation dependence, which is not simply linear due to the compressively strained quantum wells [50]. The predicted gain modulation produced by a (1001 1100) pattern for P/Q ratios of 3, 6, and 9 dB is shown in Fig. 12(e). Maximum modal gain modulations of 4.45, 2.50, and 1.33 cm^{-1} are predicted. These gain modulations produce phase fluctuations through the linewidth enhancement factor. The phase fluctuations predicted agree well with the additional chirp measured on the converted signal.

VI. Conclusion

Wavelength conversion by FWM in SOA's is the only method for wavelength conversion that provides both strict transparency and arbitrary wavelength mapping. In this paper, we have provided an update on state-of-the-art results concerning wavelength conversion at high data rates, multichannel conversion and cascaded conversion. In addition, we have tried to clarify some of the important systems issues concerning the potential application of these devices. This includes the importance of deep saturation operation of the SOA mixer, the role of pump-to-probe ratio in determining intersymbol interference in multichannel conversion, as well the characterization of parasitic chirp upon conversion in these devices. There remain many serious problems that must be overcome if these devices are ever to find use in systems. The most significant of these are: 1) the lack of a convenient means to realize polarization independent conversion (i.e., without resorting to use of dual pump waves [27]); and 2) the lack of a convenient technique for separation of the input signal and pump wave from the converted signal wave. Nonetheless, much progress has been made over the last two years on the issue of OSNR that once was considered the primary impediment to success and this bodes well for further progress on these new fronts.

Acknowledgment

The authors would like to acknowledge Ortel Corporation and Northrop-Grumman Corporation for use of important equipment. Special thanks to A. Benzoni and P.-O. Hedekvist for invaluable discussion and assistance.

References

[1] C. A. Brackett, "Is there an emerging consensus on WDM networking," *J. Lightwave Technol.*, vol. 14, pp. 936–941, 1996.
[2] S. B. Alexander, "A precompetitive consortium on wide-band all-optical networks," *J. Lightwave Technol.*, vol. 11, pp. 714–732, 1993.
[3] C. A. Brackett, "A scalable multiwavelength multihop optical network: A proposal for research on all-optical networks," *J. Lightwave Technol.*, vol. 11, pp. 736–752, 1996.
[4] J. M. Wiesenfeld, "Gain dynamics and associated nonlinearities in semiconductor optical amplifiers," in *Current Trends in Optical Amplifiers and Their Applications*, T. P. Lee, Ed. New York: World Scientific, 1996.
[5] J. M. Wiesenfeld, B. Glance, J. S. Perino, and A. H. Gnauck, "Wavelength Conversion at 10 Gb/s using a semiconductor optical amplifier," *IEEE Photon. Technol. Lett.*, vol. 5, pp. 1300–1303, 1993.
[6] T. Durhuus, B. Mikkelsen, C. Joergensen, S. L. Danielsen, and K. E. Stubkjaer, "All-optical wavelength conversion by semiconductor optical amplifiers," *J. Lightwave Technol.*, vol. 14, pp. 942–954, 1996.
[7] S. L. Danielsen, C. Jorgensen, B. Mikkelsen, P. B. Hansen, H. N. Poulsen, and K. El Stubkjaer, "Wavelength converters: Network application and systems experiments," , presented at Conf. Lasers and Electro-Optics, Baltimore, MD, May 18–23, 1997, paper CMF4.
[8] J. M. Wiesenfeld, "Wavelength conversion: Physics and devices," presented at the Conf. Lasers and Electro-Optics, Baltimore, MD, May 18–23, 1995, paper CMF1.
[9] S. J. B. Yoo, "Wavelength conversion technologies for WDM network applications," *J. Lightwave Technol.*, vol. 14, pp. 955–966, 1996.
[10] K. Inoue, "Four-wave mixing in an optical fiber in the zero-dispersion wavelength region," *J. Lightwave Technol.*, vol. 10, pp. 1553–1561, 1992.
[11] J. Zhou, N. Park, J. W. Dawson, K. J. Vahala, M. A. Newkirk, and B. I. Miller, "Terahertz four-wave mixing spectroscopy for study of ultrafast dynamics in a semiconductor optical amplifier," *Appl. Phys. Lett.*, vol. 63, pp. 1179–1181, 1993.
[12] J. Zhou, N. Park, J. W. Dawson, K. J. Vahala, M. A. Newkirk, and B. I. Miller, "Efficiency of broadband four-wave mixing wavelength conversion using semiconductor traveling-wave amplifiers," *IEEE Photon. Technol. Lett.*, vol. 6, pp. 50–52, 1994.
[13] J. Zhou, N. Park, K. J. Vahala, M. A. Newkirk, and B. I. Miller, "Four-wave mixing wavelength conversion in semiconductor traveling-wave amplifiers measured to 65 nm of wavelength shift," *IEEE Photon. Technol. Lett.*, vol. 6, pp. 984–987, 1994.
[14] M. C. Tatham, G. Sherlock, and L. D. Westbrook, "20 nm wavelength conversion using nondegenerate four-wave mixing," *IEEE Photon. Technol. Lett.*, vol. 5, pp. 1303–1306, 1993.
[15] R. Ludwig, and G. Raybon, "BER measurements of frequency converted signals using four-wave mixing in a semiconductor laser amplifier at 1, 2.5, 5, and 10 Gbit/s," *Electron. Lett.*, vol. 30, pp. 338–339, 1994.
[16] M. C. Tatham, X. Gu, L. D. Westbrook, G. Sherlock and D. M. Spirit, "Transmission of 10 Gb/s directly modulated DFB signals over 200 km standard fiber using mid-span spectral inversion," *Electron. Lett.*, vol. 30, pp. 1335–1336, 1994.
[17] R. Schnabel, U. Hilbk, Th. Hermes, P. Meissner, Cv. Helmolt, K. Magari, F. Raub, W. Pieper, F.J. Westphal, R. Ludwig, L. Kuller, and H.G. Weber, "Polariazation insensitive frequency conversion of a 10-channel OFDM signal using four-wave mixing in a semiconductor laser amplifier," *IEEE Photon. Technol. Lett.*, vol. 6, pp. 56–58, 1994.
[18] J. P. R. Lacey, S. J. Madden, M. A. Summerfield, R. S. Tucker, and A. I. Faris, "Four-channel WDM optical phase conjugator using four-wave mixing in a single semiconductor optical amplifier," *Electron. Lett.*, vol. 31, pp. 743–745, 1995.
[19] D. D. Marcenac, D. Nesset, A. E. Kelly, M. Brierly, A. D. Ellis, D. G. Moodie, and C. W. Ford, "40 Gbit/s transmission over 406 km of NDSF using mid-span spectral inversion by four-wave mixing in a 2 mm long semiconductor optical amplifier," *Electron. Lett.*, vol. 33, pp. 879–880, 1997.
[20] M. A. Summerfield and R. S. Tucker, "Noise figure and conversion efficiency of four-wave mixing in semiconductor optical amplifiers," *Electron. Lett.*, vol. 31, pp. 1159–1160, 1995.

[21] M. A. Summerfield and R. S. Tucker, "Optimization of pump and signal powers for wavelength converters based on FWM in semiconductor optical amplifiers," *IEEE Photon. Technol. Lett.*, vol. 8, pp. 1316–1318, 1996.
[22] A. D'Ottavi, F. Martelli, P. Spano, A. Mecozzi, S. Scotti, R. Dall'Ara, J. Eckner, and G, Guekos, "Very high efficiency four-wave mixing in a single semiconductor traveling-wave amplifier," *Appl. Phys. Lett.*, vol. 68, pp. 2186–2188, 1996.
[23] F. Girardin, J. Eckner, G. Guekos, R. Dall'Ara, A. Mecozzi, A. D'Ottavi, F. Martelli, S. Scotti, and P. Spano, "Low noise and very high-efficiency four-wave mixing in 1.5 mm long semiconductor optical amplifiers," *IEEE Photon. Technol. Lett.*, vol. 9, pp. 746–748, 1997.
[24] D. F. Geraghty, R. B. Lee, K. J. Vahala, M. Verdiell, M. Ziari, and A. Mathur, "Wavelength conversion up to 18 nm at 10 Gb/s by four-wave mixing in a semiconductor optical amplifier," *IEEE Photon. Technol. Lett.*, vol. 9, pp. 452–454, 1997.
[25] R. B. Lee, D. F. Geraghty, K. J. Vahala, and U. Koren, "Cascaded wavelength conversion by four-wave mixing in a strained semiconductor optical amplifier at 10 Gb/s," *IEEE Photon. Technol. Lett.*, vol. 9, pp. 752–754, 1997.
[26] D. F. Geraghty, R. B. Lee, and K. J. Vahala, "Cascaded wavelength conversions by four-wave mixing in semiconductor optical amplifiers at 10 Gb/s," in *OSA Trends in Optics and Photonics Series*. Washington, CD: Opt. Soc. Amer., vol. 12, 1997.
[27] G. Hunziker, R. Paiella, D. F. Geraghty, K. J. Vahala, and U. Koren, "Polarization-independent wavelength conversion at 2.5 Gbit/sec by dual-pump four-wave mixing in a strained semiconductor optical amplifier," *IEEE Photon. Technol. Lett.*, vol. 8, pp. 1633–1635, 1996.
[28] J. Zhou, and K. J. Vahala, "Noise reduction in FWM wavelength converters," presented at the Conf. Lasers and Electro-Optics, Baltimore, MD, May 21–26, 1995, paper CThT1.
[29] W. Shieh and A. E. Wilner, "SNR improvement of four-wave mixing wavelength shifting by noise prefiltering in a semiconductor optical amplifier," presented at the Conf. Lasers and Electro-Optics, Anaheim, CA, June 2–7, 1996, paper CThB5.
[30] K. J. Vahala, J. Zhou, D. Geraghty, R. Lee, M. Newkirk, and B. Miller, "Four-wave mixing in semiconductor traveling-wave amplifiers for wavelength conversion in all-optical networks," in *Current Trends in Optical Amplifiers and Their Applications* T. P. Lee, Ed. New York: World Scientific, 1996.
[31] G. P. Agrawal, "Population pulsations and nondegenerate four-wave mixing in semiconductor lasers and amplifiers," *J. Opt. Soc. Amer. B*, vol. 5, pp. 147–158, 1988.
[32] K. Kikuchi, M. Kakui, C.E. Zah, and T.P. Lee, "Observation of highly nondegenerate four-wave mixing in 1.5 μm traveling-wave semiconductor optical amplifiers and estimation of nonlinear gain coefficient," *IEEE J. Quantum Electron.*, vol. 28, pp. 151–156, 1992.
[33] A. Mecozzi, "Analytical theory of four-wave mixing in semiconductor amplifiers," *Opt. Lett.*, vol. 19, pp. 892–894, 1994.
[34] A. Uskov, J. Mørk, and J. Mark, "Wave mixing in semiconductor laser amplifiers due to carrier heating and spectral-hole burning," *IEEE J. Quantum Electron.*, vol. 30, pp. 1769–1781, 1994.
[35] A. Mecozzi, S. Scotti, A. D'ottavi, E. Iannone, and P. Spano, "Four-wave mixing in traveling-wave semiconductor amplifiers," *IEEE J. Quantum Electron.*, vol. 31, pp. 689–699, 1995.
[36] M. Shtaif, R. Nagar and G. Eisenstein, "Four-wave mixing among short optical pulses in semiconductor optical amplifiers," *IEEE Photon. Technol. Lett.*, vol. 7, pp. 1001–1003, 1995.
[37] I. Koltchanov, S. Kindt, K. Petermann, S. Diez, R. Ludwig, R. Schnabel, and H.G. Weber, "Gain dispersion and saturation effects in four-wave mixing in semiconductor laser amplifiers," *IEEE J. Quantum Electron.*, vol. 32, pp. 712–720, 1996.
[38] M. Shtaif and G. Eisenstein, "Noise characteristics of nonlinear semiconductor optical amplifiers in teh Gaussian limit," *IEEE J. Quantum Electron.*, vol. 32, pp. 1801–1809, 1996.
[39] I. Koltchanov, S. Kindt, K. Petermann, S. Diez, R. Ludwig, R. Schnabel, and H.G. Weber, "Analytical theory of terahertz four-wave mixing in semiconductor laser amplifiers," *Appl. Phys. Lett.*, vol. 68, pp. 2787–2789, 1996.
[40] R. Ludwig and G. Raybon, "All-optical demultiplexing using four-wave mixing in a semiconductor laser amplifier at 20 Gbit/s" presented at the Eur. Conf. Optical Communication, Montreux, Switzerland, 1993, paper ThP12.2.
[41] M. A. Summerfield, J. P. R. Lacey, A. J. Lowery, and R. S. Tucker, "All-optical TDM to WDM conversion in a semiconductor optical amplifier," *Electron. Lett.*, vol. 30, pp. 255–256, 1994.
[42] W. Shieh, E. Park, and A. E. Willner, "All-optical wavelength shifting of microwave subcarriers by using four-wave mixing in a semiconductor optical amplifier," *IEEE Photon. Technol. Lett.*, vol. 8, pp. 524–526, 1996.
[43] D. Nesset, M. Tatham, and D. Cotter, "All-optical AND gate operatingon 10 Gbit/s signals at the same waelength using four-wave mixing in a single semiconductor laser amplifier," *Electron. Lett.*, vol. 31, pp. 896–898, 1995.
[44] K. Vahala, R. Paiella, and G. Hunziker, "Ultrafast WDM logic," *IEEE J. Select. Topics Quantum Electron.*, vol. 3, pp. 698–701, Apr. 1997.
[45] A. Yariv, D. Fekete, and D. M. Pepper, "Compensation for channel dispersion by nonlinear optical phase conjugation," *Opt. Lett.*, vol. 4, pp. 52–54, 1979.
[46] S. Watanabe, T. Naito, and T. Chikama, "Compensation of chromatic dispersion in a single-mode fiber by optical phase conjugation," *IEEE Photon. Technol. Lett.*, vol. 5, pp. 92–95, 1993.
[47] R. A. Linke, "Modulation induced transient chirping in single frequency lasers," *IEEE J. Quantum Electron.*, vol. QE-21, pp. 593–597, 1985.
[48] T. L. Koch and R. A. Linke, "Effect of nonlinear gain reduction on semiconductor laser wavelength chirping," *Appl. Phys. Lett.*, vol. 48, pp. 613–615, 1986.
[49] G. P. Agrawal and N. A. Olsson, "Self-phase modulation and spectral broadening of optical pulses in semiconductor laser amplifiers," *IEEE J. Quantum Electron.*, vol. 25, pp. 2297–2305, 1989.
[50] K. J. Vahala and C. E. Zah, "Effect of doping on the optical gain and the spontaneous noise enhancement factor in quantum well amplifiers and lasers studied by simple analytical expressions," *Appl. Phys. Lett.*, vol. 52, pp. 1945–1947, 1988.

David F. Geraghty, photograph and biography not available at the time of publication.

Robert B. Lee, photograph and biography not available at the time of publication.

Marc Verdiell, photograph and biography not available at the time of publication.

Mehrdad Ziari, photograph and biography not available at the time of publication.

Atul Mathur, photograph and biography not available at the time of publication.

Kerry J. Vahala (S'82–M'84) received the Ph.D. degree in applied physics from the California Institute of Technology, Pasadena, CA, in 1985.

He is Professor of Applied Physics at CalTech. His reserach interests include semiconductor laser and fiber laser physics, high-speed dynamics in semiconductors, and semiconductor nanostructure physics and fabrication.

Dr. Vahala is a Fellow of the Optical Society of America and is currently a topical editor IEEE PHOTONICS TECHNOLOGY LETTERS and the *Journal of Semiconductor Science and Technology*. He has also served previously as topical editor for the *Journal of the Optical Society of America*. He is the first recipient of the Richard P. Feynman Hughes Fellowship and has also received both the Presidential Young Investigator Award and Office of Naval Research Young Investigator Award. In addition, he has been recognized twice by the Student Association at CalTech for excellence in teaching.